We are IntechOpen, the world's leading publisher of Open Access books Built by scientists, for scientists

6,900
Open access books available

186,000
International authors and editors

200M
Downloads

Our authors are among the

154
Countries delivered to

TOP 1%
most cited scientists

12.2%
Contributors from top 500 universities

WEB OF SCIENCE™

Selection of our books indexed in the Book Citation Index in Web of Science™ Core Collection (BKCI)

Interested in publishing with us?
Contact book.department@intechopen.com

Numbers displayed above are based on latest data collected.
For more information visit www.intechopen.com

1

Integrated Control of Vehicle System Dynamics: Theory and Experiment

Wuwei Chen[1], Hansong Xiao[2], Liqiang Liu[1],
Jean W. Zu[2] and HuiHui Zhou[1]
[1]*Hefei University of Technology,*
[2]*University of Toronto,*
P. R. China
Canada

1. Introduction

Modern motor vehicles are increasingly using active chassis control systems to replace traditional mechanical systems in order to improve vehicle handling, stability, and comfort. These chassis control systems can be classified into the three categories, according to their motion control of vehicle dynamics in the three directions, i.e. vertical, lateral, and longitudinal directions: 1) suspension, e.g. active suspension system (ASS) and active body control (ABC); 2) steering, e.g. electric power steering system (EPS) and active front steering (AFS), and active four-wheel steering control (4WS); 3) traction/braking, e.g. anti-lock brake system (ABS), electronic stability program (ESP), and traction control (TRC). These control systems are generally designed by different suppliers with different technologies and components to accomplish certain control objectives or functionalities. Especially when equipped into vehicles, the control systems often operate independently and thus result in a parallel vehicle control architecture. Two major problems arise in such a parallel vehicle control architecture. First, system complexity in physical meaning comes out to be a prominent challenge to overcome since the amount of both hardware and software increases dramatically. Second, interactions and performance conflicts among the control systems occur inevitably because the vehicle motions in vertical, lateral, and longitudinal directions are coupled in nature. To overcome the problems, an approach called integrated vehicle dynamics control was proposed around the 1990s (Fruechte et al., 1989). Integrated vehicle dynamics control system is an advanced system that coordinates all the chassis control systems and components to improve the overall vehicle performance including safety, comfort, and economy.

Integrated vehicle dynamics control has been an important research topic in the area of vehicle dynamics and control over the past two decades. Comprehensive reviews on this research area may refer to (Gordon et al., 2003; Yu et al., 2008). The aim of integrated vehicle control is to improve the overall vehicle performance through creating synergies in the use of sensor information, hardware, and control strategies. A number of control techniques have been designed to achieve the goal of functional integration of the chassis control systems. These control techniques can be classified into two categories, as suggested by (Gordon et al., 2003): 1) multivariable control; and 2) hierarchical control. Most control

techniques used in the previous studies fall into the first category. Examples include nonlinear predictive control (Falcone et al., 2007), random sub-optimal control (Chen et al., 2006), robust H_∞ (Hirano et al., 1993), sliding mode (Li et al., 2008), and artificial neural networks (Nwagboso et al., 2002), etc. In contrast, hierarchical control has not yet been applied extensively to integrated vehicle control system. It is indicated by the relatively small volume of research publications (Gordon et al., 2003; Gordon, 1996; Rodic and Vukobratovie, 2000; Karbalaei et al., 2007; He et al., 2006; Chang and Gordon, 2007; Trächtler, 2004). In the studies, there are two types of hierarchical control architecture: two-layer architecture (Gordon et al., 2003; Gordon, 1996; Rodic and Vukobratovie, 2000; Karbalaei et al., 2007; He et al., 2006) and three-layer architecture (Chang and Gordon, 2007; Trächtler, 2004). For instance in (Chang and Gordon, 2007), a three-layer model-based hierarchical control structure was proposed to achieve modular design of the control systems: an upper layer for reference vehicle motions, an intermediate layer for actuator apportionment, and a lower layer for stand-alone actuator control.

In the review of the past studies on integrated vehicle dynamics control, we address the following two aspects in this study. First, hierarchical control has been identified as the more effective control technique compared to multivariable control. In addition to improving the overall vehicle performance including safety, comfort, and economy, application of hierarchical control brings a number of benefits, among which: 1) facilitating the modular design of chassis control systems; 2) mastering complexity by masking the details of the individual chassis control system at the lower layer; 3) favoring scalability; and 4) speeding up development processes and reducing costs by sharing hardware (e.g. sensors). Second, most of the research activities on this area were focused solely on simulation investigations. There have been very few attempts to conduct experimental study to verify the effectiveness of those proposed integrated vehicle control systems. However, the experimental verification is an essential stage in developing those integrated vehicle control systems in order to transfer them from R&D activities to series production.

In this chapter, a comprehensive and intensive study on integrated vehicle dynamics control is performed. The study consists of three investigations: First, a multivariable control technique called stochastic sub-optimal control is applied to integrated control of electric power steering system (EPS) and active suspension system (ASS). A simulation investigation is performed and comparisons are made to demonstrate the advantages of the proposed integrated control system over the parallel control system. Second, a two-layer hierarchical control architecture is proposed for integrated control of active suspension system (ASS) and electronic stability program (ESP). The upper layer controller is designed to coordinate the interactions between the ASS and the ESP. A simulation investigation is conducted to demonstrate the effectiveness of the proposed hierarchical control system in improving vehicle overall performance over the non-integrated control system. Finally, a hardware-in-the-loop (HIL) experimental investigation is performed to verify the simulation results.

2. System model

In this study, two types of vehicle dynamic model are established: a non-linear vehicle dynamic model developed for simulating the vehicle dynamics, and a linear 2-DOF reference model used for designing controllers and calculating the desired responses to driver's steering input.

2.1 Vehicle dynamic model

A vehicle dynamic model is established and the three typical vehicle rotational motions, including yaw motion, pitch motion, and roll motion, are considered. They are illustrated in Fig. 1(a), Fig. 1(b), and Fig. 1(c), respectively. In the figures, we denote the front-right wheel, front-left wheel, rear-right wheel, and rear-left wheel as wheel 1, 2, 3, and 4, respectively. The equations of motion can be derived as:

For yaw motion of sprung mass shown in Fig. 1(a)

$$I_z\dot{\omega}_z - I_{xz}\ddot{\phi} = a(F_{y1} + F_{y2}) - b(F_{y3} + F_{y4}) \tag{1}$$

And the equations of motion in the longitudinal direction and the lateral direction can be written as

$$m(\dot{v}_x - v_y\omega_z) - m_s h\dot{\omega}_z\phi = F_{x1} + F_{x2} + F_{x3} + F_{x4} - f_r mg \tag{2}$$

$$m(\dot{v}_y + v_x\omega_z) + m_s h\ddot{\phi} = F_{y1} + F_{y2} + F_{y3} + F_{y4} \tag{3}$$

For pitch motion of sprung mass shown in Fig. 1(b)

$$I_y\ddot{\theta} = b(F_{z3} + F_{z4}) - a(F_{z1} + F_{z2}) \tag{4}$$

And for roll motion of sprung mass shown in Fig. 1(c)

$$I_x\ddot{\phi} + m_s(\dot{v}_y + \dot{v}_x\omega_z)h - I_{xz}\dot{\omega}_z = m_s gh\phi + (F_{z2} + F_{z3} - F_{z1} - F_{z4})d \tag{5}$$

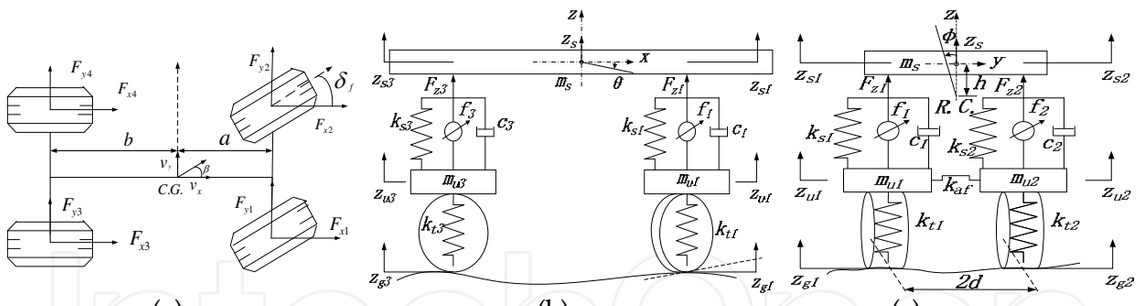

Fig. 1. Three typical vehicle rotational motions: (a) yaw motion; (b) pitch motion; (c) roll motion.

We also have the equations for the vertical motions of sprung mass and unsprung mass

$$m_s\ddot{z}_s = F_{z1} + F_{z2} + F_{z3} + F_{z4} \tag{6}$$

$$m_{ui}\ddot{z}_{ui} = k_{ti}(z_{gi} - z_{ui}) - F_{zi} \qquad (i=1,2,3,4) \tag{7}$$

where

$$F_{z1} = k_{s1}(z_{u1} - z_{s1}) + c_1(\dot{z}_{u1} - \dot{z}_{s1}) - \frac{k_{af}}{2d}[\phi - \frac{(z_{u2} - z_{u1})}{2d}] + f_1 \tag{8}$$

$$F_{z2} = k_{s2}(z_{u2} - z_{s2}) + c_2(\dot{z}_{u2} - \dot{z}_{s2}) + \frac{k_{af}}{2d}[\phi - \frac{(z_{u2} - z_{u1})}{2d}] + f_2 \tag{9}$$

$$F_{z3} = k_{s3}(z_{u3} - z_{s3}) + c_3(\dot{z}_{u3} - \dot{z}_{s3}) + \frac{k_{ar}}{2d}[\phi - \frac{(z_{u3} - z_{u4})}{2d}] + f_3 \tag{10}$$

$$F_{z4} = k_{s4}(z_{u4} - z_{s4}) + c_4(\dot{z}_{u4} - \dot{z}_{s4}) - \frac{k_{ar}}{2d}[\phi - \frac{(z_{u3} - z_{u4})}{2d}] + f_4 \tag{11}$$

When the pitch angle of sprung mass θ and the roll angle of sprung mass ϕ are small, the following approximation can be reached

$$z_{s1} = z_s - a\theta - d\phi \tag{12}$$

$$z_{s2} = z_s - a\theta + d\phi \tag{13}$$

$$z_{s3} = z_s + b\theta + d\phi \tag{14}$$

$$z_{s4} = z_s + b\theta - d\phi \tag{15}$$

Considering the rotational dynamics of the wheel of the vehicle shown in Fig. 2, the equation of motion is derived as

$$I_w\dot{\omega}_i = -F_{xwi}R_w + T_i \qquad (i = 1,\ldots 4) \tag{16}$$

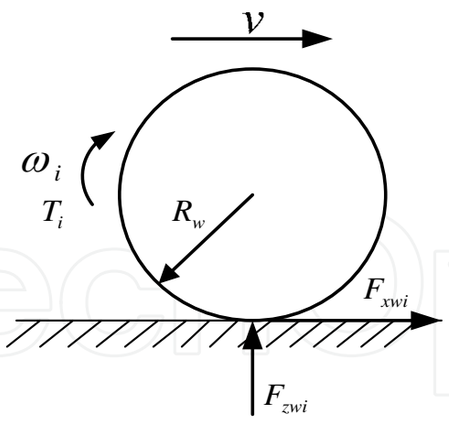

Fig. 2 Wheel dynamic model.

It is noted that the longitudinal and lateral forces acting on the *i*-th wheel, F_{xi} and F_{yi}, have the following relationships with the tyre forces along the wheel axes, F_{xwi} and F_{ywi}, because of the steering angle of the *i*-th wheel δ_i,

$$\begin{bmatrix} F_{xi} \\ F_{yi} \end{bmatrix} = \begin{bmatrix} \cos\delta_i & \sin\delta_i \\ \sin\delta_i & -\cos\delta_i \end{bmatrix} \begin{bmatrix} F_{xwi} \\ F_{ywi} \end{bmatrix} \qquad (i = 1,\ldots,4) \tag{17}$$

For simplicity, the steering angles are assumed as: $\delta_1 = \delta_2 = \delta_f$, and $\delta_3 = \delta_4 = \delta_r$.

It is worthy to mention that: 1) for the above-mentioned first investigation, both the ASS controller and EPS controller are designed respectively. Eq. 4 through Eq. 15 are used to develop the ASS controller, while the other equations are employed to design the EPS controller; 2) for the second investigation, the same set of equations, i.e. Eq. 4 through Eq. 15, is used to design the ASS controller. While for the ESP controller, the yaw motion of sprung mass described in Eq. 1 is replaced by the following equations of motion.
For yaw motion of sprung mass

$$I_z\dot{\omega}_z - I_{xz}\ddot{\phi} = a(F_{y1} + F_{y2}) - b(F_{y3} + F_{y4}) + M_{zc} \tag{18}$$

where M_{zc} is the corrective yaw moment generated by the ESP controller, which is given as

$$M_{zc} = d(F_{x1} + F_{x3} - F_{x2} - F_{x4}) \tag{19}$$

2.2 EPS model

The major components of a rack-pinion EPS as shown in Fig. 3 consist of a torque sensor, a control unit (ECU), a motor, and a gear assist mechanism. The torque sensor measures the torque from the steering wheel and sends a signal to the ECU. The ECU also receives steering position signal from a position sensor and the vehicle speed signal. These signals are processed in the ECU and an assist command is generated. The command is in turn given to the motor, which provides the torque to the gear assist mechanism. The torque is amplified by the gear mechanism and the amplified torque is applied to the steering column, which is connected to the rack-pinion mechanism.

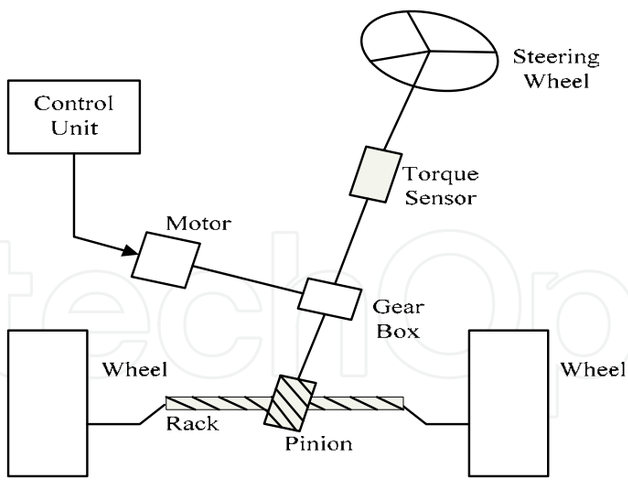

Fig. 3. EPS system.

The following governing equations for the pinion can be obtained by applying force analysis to the pinion

$$I_p\ddot{\delta}_1 = T_m + T_c - T_r - c_e\dot{\delta}_1 \tag{20}$$

where T_c is the torque applied on the steering wheel, which can be calculated by

$$T_c = k_s(\theta_h - \delta_1) \tag{21}$$

Let the speed reduction ratio of the rack-pinion mechanism be N_2, we have

$$\delta_1 = N_2\delta_f \tag{22}$$

2.3 Tyre model

The Pacejka nonlinear tyre model (Bakker et al., 1987; Pacejka, 2002) is used to determine the dynamic forces of each tyre *i*. The inputs of the tyre model include the vertical tyre force, tyre sideslip angle and tyre slip ratio; and the outputs include the longitudinal tyre force F_{xwi}, lateral tyre force F_{ywi} and self-aligning torque T_{zwi}. The Pacejka's magic formula is presented as

$$F_{xwi} = -(\sigma_x / \sigma)F_{x0} \tag{23}$$

$$F_{ywi} = -(\sigma_y / \sigma)F_{y0} \tag{24}$$

$$T_{zwi} = D_z \sin\left[C_z \tan^{-1}(B_z\phi_z)\right] \tag{25}$$

where T_{zwi} is the aligning torque acting on the tyre; and

$$F_{x0} = D_x \sin\left[C_x \tan^{-1}(B_x\phi_x)\right] \tag{26}$$

$$F_{y0} = D_y \sin\left[C_y \tan^{-1}(B_y\phi_y)\right] \tag{27}$$

$$\sigma = \sqrt{{\sigma_x}^2 + {\sigma_y}^2}\ ,\ \sigma_x = -\lambda/(1+\lambda)\ ,\ \sigma_y = -\tan\alpha/(1+\lambda) \tag{28}$$

where the coefficients depend on the tyre characteristics and road conditions, the physical definitions of these coefficients can be found in the references (Bakker et al., 1987; Pacejka, 2002).

2.4 Road excitation model

A filtered white noise signal (Yu and Crolla, 1998) is selected as the road excitation to the vehicle, which can be expressed as

$$\dot{z}_{g\,i} = -2\pi f_0 z_{g\,i} + 2\pi w_i\sqrt{G_0 v} \qquad (i = 1,\ldots,4) \tag{29}$$

2.5 2-DOF vehicle rreference model

A 2-DOF linear bicycle model is used as the vehicle reference model to generate the desired vehicle states in this study since the 2-DOF model reflects the desired relationship between the driver's steer input and the vehicle yaw rate. This model is employed for both the upper layer controller design and the ESP controller design later in the paper. The equations of motion are expressed as follows by assuming a small sideslip angle and a constant forward speed.

$$m(\dot{v}_y + v_x\omega_z) = C_f(\beta + \frac{a\omega_z}{v_x} - \delta_f) + C_r(\beta - \frac{b\omega_z}{v_x}) \tag{30}$$

$$I_z\dot{\omega}_z = aC_f(\beta + \frac{a\omega_z}{v_x} - \delta_f) - bC_r(\beta - \frac{b\omega_z}{v_x}) + M_{zc} \tag{31}$$

3. Investigation 1: Multivariable control

As mentioned earlier in the chapter, the first investigation addresses the coupling effects between dynamics of the steering system and the suspension system. With this in mind, a full-car dynamic model that integrates EPS and ASS is established. Then based on the integrated model, a multivariable control method called stochastic sub-optimal control strategy based on output feedback is applied to coordinate the control of both EPS and ASS.

3.1 State space formulation

For further analysis, it is convenient to formulate the full car dynamic model in state space form by combining the dynamic models for the sub-systems that we developed earlier in Section 2. Firstly, the state variables are defined as

$$X = \left[\dot{\delta} \quad \delta \quad \beta \quad \omega_z \quad \dot{\theta} \quad \theta \quad \dot{z}_{u1} \quad \dot{z}_{u2} \quad \dot{z}_{u3} \quad \dot{z}_{u4}\, z_{u1} \quad z_{u2} \quad z_{u3} \quad z_{u4} \quad \dot{\phi} \quad \phi \quad \dot{z}_s \quad z_s \quad z_{g1} \quad z_{g2} \quad z_{g3} \quad z_{g4}\right]^T \tag{32}$$

and the output variables are chosen as

$$Y = \left[\delta \quad T_C \quad \beta \quad \omega_z \quad \dot{\phi} \quad \dot{z}_s \quad \dot{\theta} \quad z_{u1} - z_{s1} \; z_{u2} - z_{s2} \quad z_{u3} - z_{s3} \quad z_{u4} - z_{s4} \quad k_{t1}\left(z_{g1} - z_{u1}\right) k_{t2}\left(z_{g2} - z_{u2}\right) \quad k_{t3}\left(z_{g3} - z_{u3}\right) \quad k_{t4}\left(z_{g4} - z_{u4}\right)\right]^T \tag{33}$$

where $z_{ui} - z_{si}$ represents the suspension dynamic deflection at wheel *i*, and $k_{ti}\left(z_{gi} - z_{ui}\right)$ represents the tyre dynamic load at wheel *i*. Therefore the state equation and output equation can be written as

$$\begin{cases} \dot{X}(t) = AX(t) + B_1U(t) + B_2U_2(t) + B_3W(t) \\ Y(t) = CX(t) \end{cases} \tag{34}$$

where $U(t)$ is the control input vector, and $U(t) = [T_m(t) \quad f_1(t) \quad f_2(t) \quad f_3(t) \quad f_4(t)]^T$; $U_2(t)$ is the steering input vector, and $U_2(t) = \left[\theta_h(t)\right]^T$; $W(t)$ is the Gaussian white noise disturbance input vector, and $W(t) = [w_1(t) \quad w_2(t) \quad w_3(t) \quad w_4(t)]^T$.

3.2 Integrated controller design

The stochastic sub-optimal control strategy based on output feedback is applied to design the integrated controller. This control strategy monitors the vehicle states and adjusts or tunes the control forces for the ASS and the assist torque for the EPS by using the measured outputs. The major advantage of the algorithm is that the critical parameters suggested by the original dynamic system are automatically adjusted by the sub-optimal feedback law. This overcomes the disadvantage resulted from that some of the state variables are immeasurable in practice. To apply the control strategy, we first propose the objective function (or performance indices) for the integrated control system defined in Eq. 34.

Since it is a full-car dynamic model that integrates EPS and ASS, the multiple vehicle performance indices must be considered, which include maneuverability, handling stability, ride comfort, and safety. These performance indices can be measured by the following physical terms: the torque applied on the steering wheel T_c, the yaw rate of the full car ω_z, the pitch angle of sprung mass θ, the roll angle of sprung mass ϕ, the vertical acceleration of sprung mass $\ddot{z}_s$, the suspension dynamic deflection $z_s - z_u$, and the tyre dynamic load $k_t(z_u - z_g)$. In addition, we also take into account the consumed control energy, which is represented by the assist torque T_m and the control force of the active suspension f_i. Therefore, the integrated performance index is defined as

$$\begin{aligned} \boldsymbol{J} = \boldsymbol{E}\Big\{ \int_0^\infty [&q_1(T_c - T_0)^2 + q_2\omega_z{}^2 + q_3\dot{\phi}^2 + q_4\ddot{z}_s{}^2 + q_5\dot{\theta}^2 + q_6(z_{u1} - z_{s1})^2 + \\ &q_7(z_{u2} - z_{s2})^2 + q_8(z_{u3} - z_{s3})^2 + q_9(z_{u4} - z_{s4})^2 + q_{10}\left(k_{t1}(z_{g1} - z_{u1})\right)^2 + \\ &q_{11}\left(k_{t2}(z_{g2} - z_{u2})\right)^2 + q_{12}\left(k_{t3}(z_{g3} - z_{u3})\right)^2 + q_{13}\left(k_{t4}(z_{g4} - z_{u4})\right)^2 + r_m T_m{}^2 + \\ &r_1 f_1^2 + r_2 f_2^2 + r_3 f_3^2 + r_4 f_4^2]dt \Big\} \end{aligned} \tag{35}$$

where $q_1, \cdots, q_{13}$, r_m, $r_1 \cdots, r_4$ are the weighting coefficients. We rewrite Eq. 35 in matrix form

$$\begin{aligned} \boldsymbol{J} &= E\left\{ \int_0^\infty \left[Y^T Q_0 Y + U^T R U \right] dt \right\} = E\left\{ \int_0^\infty \left[X^T \left(C^T Q_0 C \right) X + U^T R U \right] dt \right\} \\ &= E\left\{ \int_0^\infty \left[X^T Q X + U^T R U \right] dt \right\} \end{aligned} \tag{36}$$

where $Q = C^{\mathrm{T}} Q_0 C$; $\boldsymbol{Q}_0 = diag\{q_1, q_2, \cdots, q_{13}\}$; $R = diag\{r_1, r_2, r_3, r_4, r_{\mathrm{m}}\}$.

To minimize the above performance index, the sub-optimal feedback control law is developed as follows.

The control matrix $\boldsymbol{U}$ can be expressed by

$$U = -KY \tag{37}$$

where $\boldsymbol{K}$ is the output feedback gain matrix, which can be derived through the following procedure.

Step 1. We first can derive the state feedback gain matrix F^* using optimal control method:

$$F^* = R^{-1} B^T P \tag{38}$$

where the matrix $\boldsymbol{B}$ is calculated as $B = A A_1^{-1} B_1$; and the matrix $\boldsymbol{P}$ is the solution of the following *Riccati* equation:

$$PA + A^T P - PBR^{-1} B^T P + Q = 0 \tag{39}$$

Step 2. Since there is no inverse matrix for the non-square (or rectangular) matrix $\boldsymbol{C}$, the output feedback gain matrix $\boldsymbol{K}$ cannot be directly obtained through the equation $KC = F^*$. In

this case, the norm-minimizing method is used to find the approximate solution of $\boldsymbol{K}$ (Gu et al., 1997). First, the following objective function is constructed

$$H = \left\| F - F^* \right\| = \sqrt{\sum_{i=1}^{22} \sum_{j=1}^{22} \left(F_{ij}^* - F_{ij} \right)^2} \tag{40}$$

and then we can find $\boldsymbol{F}$ by minimizing the objective function $\boldsymbol{H}$

$$F = F^* C^T \left(CC^T \right)^{-1} C \tag{41}$$

we also have

$$F = KC \tag{42}$$

Thus $\boldsymbol{K}$ is derived by combining Eq. 41 and Eq. 42

$$K = F^* C^T \left(CC^T \right)^{-1} \tag{43}$$

and the control matrix $\boldsymbol{U}$ becomes

$$U = -KY = -F^* C^T \left(CC^T \right)^{-1} Y \tag{44}$$

3.3 Simulations and discussions

The integrated control system is analyzed using Matlab/Simulink. We assume that the vehicle travels at a constant speed v_x = 20m/s, and is subject to a steering input from steering wheel. The steering input is set as a step signal with amplitude of 120°.

The road excitation shown in Fig. 4 is assumed to be independent for each wheel and the power of the white noise for each wheel equals 20dB. The assumption of independent road excitation for each wheel has practical significance because in real road conditions, the road excitations on the four wheels of the vehicle are different and independent. It must be noted that this assumption on the road excitation is different from the assumption commonly made in other studies. The commonly made assumption states that the rear wheels follow the front wheels on the same track and hence the excitations at the rear wheels are just the same as the front wheels except for a time lag. Such a simplification is not applied in this simulation. The values of the vehicle physical parameters used in the simulation are listed in Table 1.

The parameter setting for the weighting coefficient matrices $\boldsymbol{Q}_0$ and $\boldsymbol{R}$ defined in Eq. 36 plays an important role in the simulation performance. After tuning these weighting coefficients, we choose the following parameter setting when a satisfactory system performance is achieved: $q_1 = 10$, $q_2 = 10^6$, $q_3 = 5.0 \times 10^5$, $q_4 = q_5 = 2 \times 10^6$, $q_6 = q_7 = \cdots = q_{13} = 10^3$, $r_m = 0.1$, and $r_1 = r_2 = r_3 = r_4 = 1$.

It must be noted that different levels of importance are assigned to the different performance indices with such a parameter setting for the weighting coefficients. For example, the vertical acceleration of sprung mass is considered to be more important than the suspension dynamic deflection. In order to study comprehensively the characteristics of

N_2	20	c_3/c_4	1760/ 1760 (N·s/m)
k_s	90 (N·m/ rad)	k_t	138000 (N/m)
I_p	0.06 (kg·m^2)	h	0.505 (m)
c_e	0.3 (N·s·m/rad)	d	0.64 (m)
M	1030 (kg)	a	0.968 (m)
m_s	810 (kg)	b	1.392 (m)
m_{u1}/m_{u2}	26.5/ 26.5 (kg)	I_x	300 (kg·m^2)
m_{u3}/m_{u4}	24.4/ 24.4 (kg)	I_y	1058.4 (kg·m^2)
k_{s1}/k_{s2}	20600/ 20600 (N/m)	I_z	1087.8 (kg·m^2)
k_{s3}/k_{s4}	15200/ 15200 (N/m)	f_0	0.01 (Hz)
k_{af}/k_{ar}	6695/ 6695 (N·m/ rad)	G_0	5.0×10^{-6} (m^3/cycle)
c_1/c_2	1570/ 1570 (N·s/m)	v_x	20m/s

Table 1. Vehicle Physical Parameters.

the integrated control system, the integrated control system is compared to two other systems. One is the system without control, i.e. the passive mechanical system. While the other is the system that only has ASS (denoted as ASS-only) or EPS (denoted as EPS-only). For each of the two control systems, the sub-optimal control strategy is applied and the identical parameter setting for the weighting coefficient matrices $\boldsymbol{Q}_0$ and $\boldsymbol{R}$ is selected.

It can be observed from the simulation results that all the performance indices are improved for the integrated control system, compared to those for the passive system, and those for ASS-only or EPS-only. For brevity, only the performance indices with higher lever of importance are selected to illustrate in Fig. 5 through Fig. 8. The following discussions are made:

1. As shown in Fig. 5, the roll angle for the integrated control system is reduced significantly compared to that for the ASS-only system and the passive system. A quantitative analysis of the results shows that the peak value of the roll angle for the integrated control system is decreased by 37.6%, compared to that for the ASS-only system, and 55.3% for the passive system. Moreover, the roll angle for the integrated control is damped quickly and thus less oscillation is observed for the integrated control system, compared to the other two systems. Therefore the results indicate that the anti-roll ability of the vehicle is greatly enhanced and thus a better handling stability is achieved through the application of the integrated control system.
2. It is presented clearly in Fig. 6 that the overshoot of the yaw rate for the integrated control system is decreased compared to that for the EPS-only system and the passive system. Furthermore, the yaw rate for the integrated control system and the EPS-only system becomes stable more quickly than the passive system after the overshoot. However, there is no significant time difference for the integrated control system and the EPS-only system to stabilize the yaw rate after the overshoot. The results demonstrate that the application of the integrated control system contributes a better lateral stability to the vehicle, compared to the EPS-only system and the passive system.
3. A quantitative analysis is performed for the vertical acceleration of sprung mass as shown in Fig. 7. The obtained R.M.S. (Root-Mean-Square) value of the vertical acceleration of sprung mass for the integrated control system is reduced by 23.1%,

compared to that for the ASS-only system, and 35.5% for the passive system. The results show that the vehicle equipped with the integrated control system has a better ride comfort than that with the ASS-only system and the passive system. In addition, the dynamic deflection of the front suspension as shown in Fig. 8 also suggests similar results.

In summary, the integrated control system improves the overall vehicle performance including handling, lateral stability, and ride comfort, compared to either the EPS-only system or the ASS-only system, and the passive system.

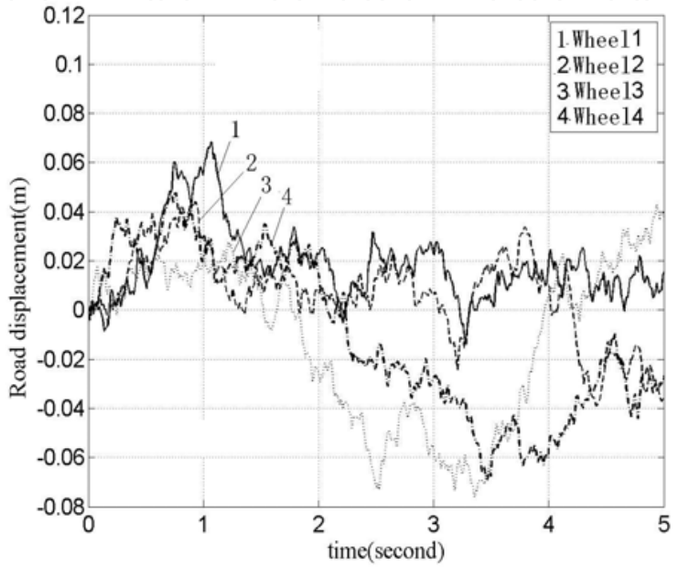

Fig. 4. Road Input.

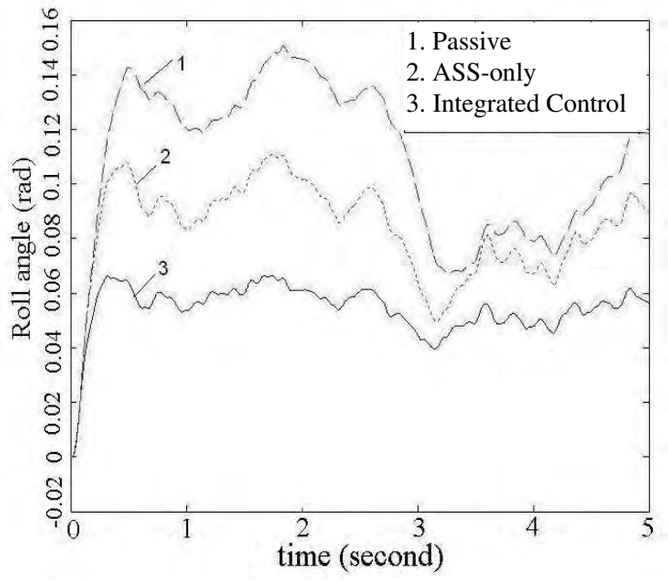

Fig. 5. Roll angle.

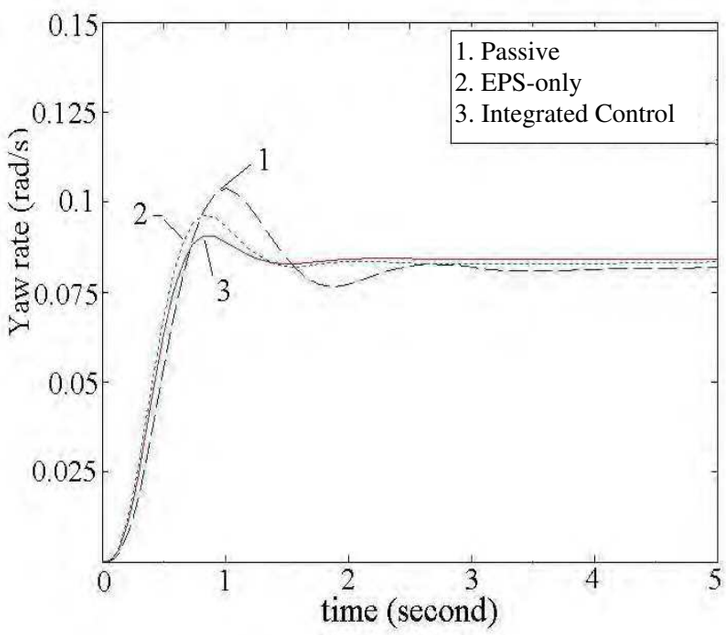

Fig. 6. Yaw rate.

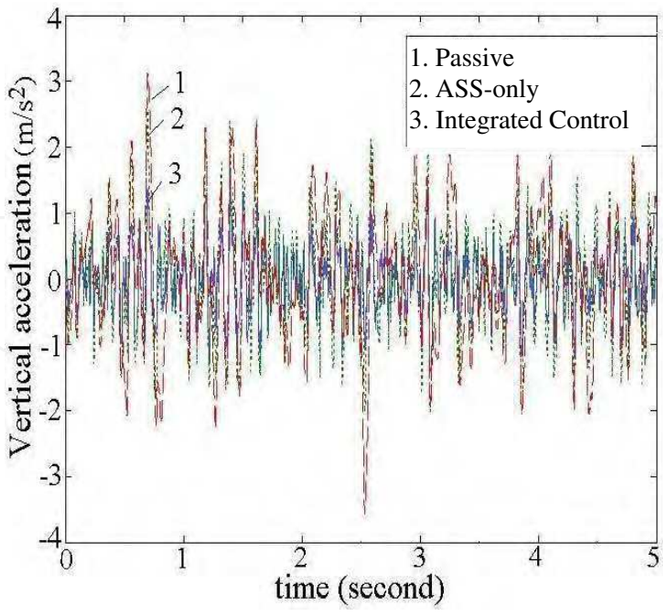

Fig. 7. Vertical acceleration of sprung mass.

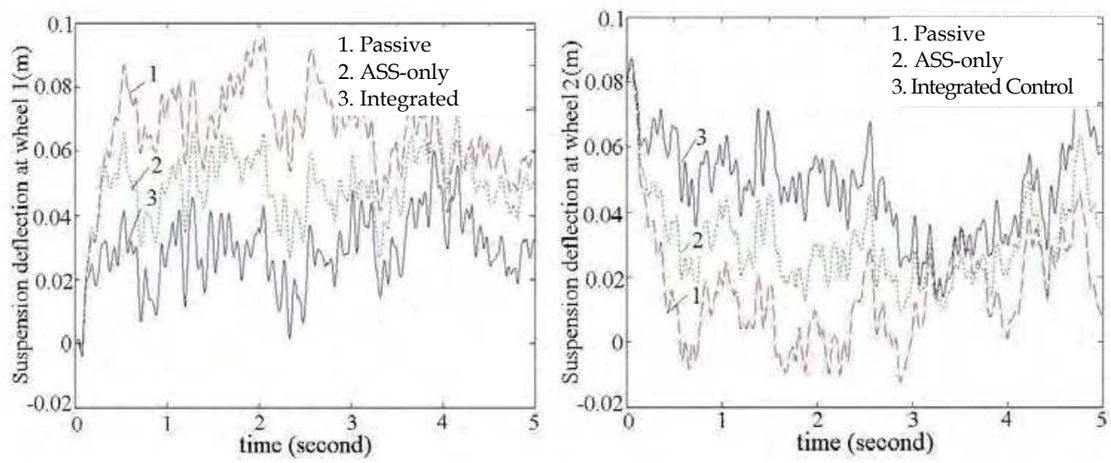

(a) (b)

Fig. 8. Front suspension deflection: (a) at wheel 1; (b) at wheel 2.

In this investigation, a full-car dynamic model has been established through integrating electrical power steering system (EPS) with active suspension system (ASS) in order to address the coupling effects between the dynamics of the steering system and the suspension system. Thereafter, a multivariable control approach called stochastic sub-optimal control strategy based on output feedback has been applied to coordinate the control of both the EPS and ASS. Simulation results show that the integrated control system is effective in fulfilling the integrated control of the EPS and the ASS. This is demonstrated by the significant improvement on the overall vehicle performance including handling, lateral stability, and ride comfort, compared to either the EPS-only system or the ASS-only system, and the passive system. However, the development of the integrated vehicle control system requires fully understanding the vehicle dynamics in both the global level and system or subsystem level. Thus the development task for the integrated vehicle control system becomes very difficulty when the number of control systems increases. Furthermore, a whole new design is required for the integrated vehicle control system including both control logic and hardware, when a new control system, e.g. anti-lock brake system (ABS), is equipped with.

4. Investigation 2: Hierarchical control

In the above investigation, we demonstrated the effectiveness of one of the integrated control approaches called multivariable control on coordinating the control of the ASS and the EPS. While the second investigation moves up a step further on developing the integrated control approach. To this end, a hierarchical control architecture is proposed for integrated control of active suspension system (ASS) and electronic stability program (ESP). The advantages of the hierarchical control architecture are demonstrated through the following design practice of the integrated control system.

4.1 Hierarchical controller design

The architecture of the proposed hierarchical control system is shown in Fig. 9. The control system consists of two layers. The upper layer controller monitors the driver's intentions

and the current vehicle states including the steering angle of the front wheel δ_f, the sideslip angle β, the yaw rate ω_z and the lateral acceleration a_y, etc. Based on these input signals, the upper layer controller computes the corrective yaw moment M_{zc} in order to track the desired vehicle motions. Thereafter, the upper layer controller generates the distributed torques M_{ESP} and M_{ASS} to the two lower layer controllers, i.e., the ESP and the ASS, respectively, according to a rule-based control strategy. Moreover, the distributed torques M_{ESP} and M_{ASS} are converted into the corresponding control commands for the two individual lower layer controllers. Finally, the ESP and the ASS execute respectively their local control objectives to control the vehicle dynamics. The upper layer controller and the two lower layer controllers are designed as follows.

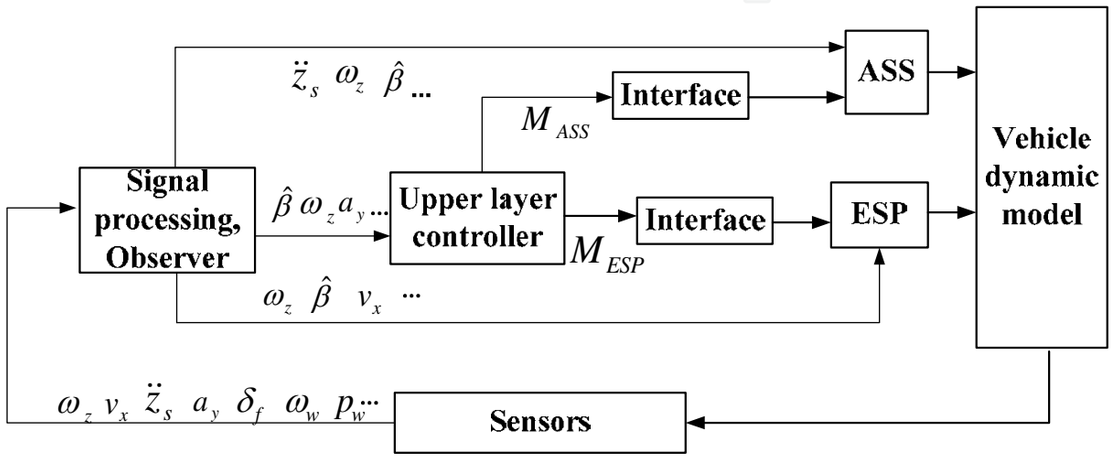

Fig. 9. Block diagram of the hierarchical control system.

4.2 Upper layer controller design

It is known that both the applications of the ESP and the ASS are able to develop corrective yaw moments (either directly or indirectly). To coordinate the interactions between the ASS and the ESP, a simple rule-based control strategy is proposed to design the upper layer controller. The aim of the proposed control rule is to distribute the corrective yaw moment appropriately between the two lower layer controllers. The control rule is described as follows.

First, the corrective yaw moment M_{zc} is calculated by using the 2-DOF vehicle reference model defined in Section 2.5, based on the measured and estimated vehicle input signals.

Second, the braking/traction torque M_d and the pitch torque M_p are computed by using the following equations

$$M_d = c_p \cdot p_w - 0.5 M_{zc} + I_w \cdot \dot{\omega}_w \tag{45}$$

$$M_p = \frac{k_\alpha tan\alpha}{c_\lambda \lambda_w} M_d \tag{46}$$

where Eq. (45) is derived by considering the dynamics of one of the front wheels. It should be noted that although a front wheel drive vehicle is assumed, the main conclusions of this

study can be easily extended to vehicles with other driveline configurations; In general, the brake torque at each wheel is a function of the brake pressure p_w at that wheel, and c_p is an equivalent braking coefficient of the braking system, which is determined by using the equation $c_p = A_w \mu_b R_b$; The number "0.5" represents that the corrective yaw moment is evenly shared by the two front wheels.

Finally, the distributed torques M_{ESP} and M_{ASS} are generated by using a linear combination of the braking/traction torque M_d and the pitch torque M_p, which is given as

$$\begin{cases} M_{ESP} = n_1 M_d + (1 - n_1) M_p \\ M_{ASS} = n_2 M_p + (1 - n_2) M_d \end{cases} \tag{47}$$

where n_1 and n_2 are the weighting coefficients, and $1 > n_1 > 0.5$, $1 > n_2 > 0.5$. Therefore, through tuning the weighting coefficients n_1 and n_2, the upper layer controller is able to coordinate the two lower layer controllers and determine to what extent the two lower layer controllers to be controlled.

4.3 Lower layer controller design

4.3.1 ASS controller design

The LQG control method is used to control the active suspension system. The state variables are defined as $X = [z_s \;\; \dot{z}_s \;\; z_{u1} \;\; z_{u2} \;\; z_{u3} \;\; z_{u4} \;\; \dot{z}_{u1} \;\; \dot{z}_{u2} \;\; \dot{z}_{u3} \;\; \dot{z}_{u4} \;\; \theta \;\; \phi \;\; \dot{\theta} \;\; \dot{\phi}]^{\mathrm{T}}$; and the output variables are chosen as $Y = [\ddot{z}_s \;\; z_{u1} \;\; z_{u2} \;\; z_{u3} \;\; z_{u4} \;\; \theta \;\; \varphi]^{\mathrm{T}}$. Therefore, based on Eq. 4 through Eq. 16, together with the road excitation model presented in Section 2.4, the state equation and the output equation can be written as

$$\begin{cases} \dot{X} = AX + BU \\ Y = CX + DU \end{cases} \tag{48}$$

where $U = [U_1 \;\; U_2]^{\mathrm{T}}$ is the control input vector. $U_1 = [f_1 \;\; f_2 \;\; f_3 \;\; f_4]^{\mathrm{T}}$ is the control force vector, and $U_2 = [z_{g1} \;\; z_{g2} \;\; z_{g3} \;\; z_{g4}]^{\mathrm{T}}$ is the road excitation vector. The multiple vehicle performance indices are considered to evaluate the vehicle handling stability, ride comfort, and safety. These performance indices can be measured by the following physical terms: vertical displacement of each wheel z_{u1}, z_{u2}, z_{u3}, z_{u4}; the suspension dynamic deflections $(z_{s1} - z_{u1})$, $(z_{s2} - z_{u2})$, $(z_{s3} - z_{u3})$, $(z_{s4} - z_{u4})$; the vertical acceleration of sprung mass $\ddot{z}_s$; the pitch angular acceleration $\ddot{\theta}$; the roll angular acceleration $\ddot{\varphi}$; and the control forces of the active suspension f_1, f_2, f_3, f_4. Therefore, the combined performance index is defined as

$$\begin{aligned} J = \lim_{T \to \infty} \frac{1}{T} \int_0^T [& q_1 z_{u1}^2 + q_2 z_{u2}^2 + q_3 z_{u3}^2 + q_4 z_{u4}^2 + q_5 (z_{s1} - z_{u1})^2 \\ & + q_6 (z_{s2} - z_{u2})^2 + q_7 (z_{s3} - z_{u3})^2 + q_8 (z_{s4} - z_{u4})^2 + q_9 \ddot{\theta}^2 \\ & + q_{10} \ddot{\phi}^2 + q_{11} \ddot{z}_s^2 + r_1 f_1^2 + r_2 f_2^2 + r_3 f_3^2 + r_4 f_4^2] dt \end{aligned} \tag{49}$$

where $q_1,\ldots,q_{11}$, and $r_1,\ldots,r_4$ are the weighting coefficients. The above equation can be rewritten as the following matrix form

$$J = \lim_{T\to\infty} \frac{1}{T}\int_0^T (X^T QX + U^T RU + 2X^T NU)dt \tag{50}$$

where Q, R, N are the weighting matrices.

The state feedback gain matrix K is derived using the optimal control method, and it is the solution of the following *Riccati* equation

$$KA + A^T K + Q - KB_1 R^{-1} B_1{}^T K + B_2 U_2 B_2{}^T = 0 \tag{51}$$

4.3.2 ESP controller design

In this study, an adaptive fuzzy logic (AFL) method is applied to the design of the ESP controller. Fuzzy logic controller (FLC) has been identified as an attractive control method in vehicle dynamics control (Boada et al., 2005). This method has advantages when the following situations are encountered: 1) there is no explicit mathematical model that describes how control outputs functionally depend on control inputs; 2) there are experts who are able to incorporate their knowledge into the control decision-making process. However, traditional FLC with a fixed parameter setting cannot adapt to changes in the vehicle operating conditions or in the environment. Therefore, an adaptive mechanism must be introduced to adjust the controller parameters in order to achieve a satisfactory vehicle performance in a wide range of changing conditions.

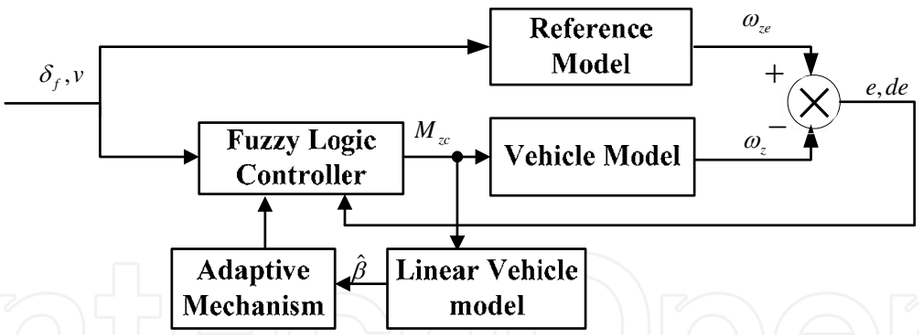

Fig. 10. Block diagram of the adaptive fuzzy logic controller for ESP.

As shown in Fig. 10, the AFL controller consists of a FLC and an adaptive mechanism. To design the AFL controller, the yaw rate and the sideslip angle of the vehicle are selected as the control objectives. The yaw rate can be measured by a gyroscope, but the sideslip angle cannot be directly measured and thus has to be estimated by an observer. The observer is designed by using the 2-DOF vehicle model described in Section 2.4. The linearized state space equation of the 2-DOF vehicle model is derived as follows, with the assumptions of a constant forward speed and a small sideslip angle.

$$\begin{cases} \dot{X} = A_E \cdot X + B_E \cdot U \\ Y = C_E \cdot X + D_E \cdot U \end{cases} \tag{52}$$

where

$$X=\begin{bmatrix}\beta\\ \omega_z\end{bmatrix},\ U=\begin{bmatrix}\delta_f\\ M_{zc}\end{bmatrix},\ A_E=\begin{bmatrix}-\frac{C_f+C_r}{mv} & -1-\frac{aC_f-bC_r}{mv^2}\\ -\frac{aC_f-bC_r}{I_z} & -\frac{a^2C_f+b^2C_r}{I_zv}\end{bmatrix},\ B_E=\begin{bmatrix}\frac{C_f}{mv} & 0\\ \frac{aC_f}{I_z} & \frac{1}{I_z}\end{bmatrix},\ C_E=\begin{bmatrix}1 & 0\\ 0 & 1\end{bmatrix},$$

$$D_E=\begin{bmatrix}0 & 0\\ 0 & 0\end{bmatrix}.$$

The aim of the AFL is to track both the desired yaw rate and the desired sideslip angle. The desired yaw rate is calculated as

$$\omega_{ze}=\frac{v_x\cdot\delta_f}{L\cdot(1+S\cdot v_x^2)} \tag{53}$$

where L is the wheel base; S is the stability factor of the vehicle, and $S=m(b/C_f-a/C_r)/L^2$. As shown in Fig. 10, the FLC has two input variables, the tracking error of the yaw rate e and the difference of the error de. They are defined as, at the kth sampling time

$$e(k)=\omega_z(k)-\omega_{ze}(k) \tag{54}$$

$$de(k)=e(k)-e(k-1) \tag{55}$$

The output variable of the FLC is defined as the corrective yaw moment M_{zc}. To determine the fuzzy controller output for the given error and its difference, the decision matrix of the linguistic control rules is designed and presented in Table 2. These rules are determined based on expert knowledge and a large number of simulation results performed in the study. In designing the FLC, the scaling factors k_e and k_{de} have great effects on the performance of the controller. Therefore the adaptive mechanism is applied to adjust the parameters in order to achieve a satisfactory control performance when there are changes in the vehicle operating conditions or in the environment. The adaptive law is given as

$$\beta(k_e)=\beta_0+k_e\int_0^t(\frac{a_y}{v}-\omega_z)dt \tag{56}$$

$$\dot{\beta}(k_{de})=-\omega_z+k_{de}\frac{1}{v}(a_y cos\beta-a_x sin\beta) \tag{57}$$

where $\beta_0=0$. Full details of the derivation of the above equations are given in the Appendix.

4.4 Simulations and discussions

In order to evaluate the performance of the developed hierarchical control system, a simulation investigation is performed. The performance and dynamic behaviors of the hierarchical control system are analyzed using Matlab/Simulink. We assume that the vehicle travels at a constant speed v = 90 km/h. Two driving conditions are performed: 1) step steering input; and 2) double lane change. For the first case, the vehicle is subject to a

de / *e*	PB	PM	PS	O	NS	NM	NB
PB	NB	NB	NB	NB	NM	O	O
PM	NB	NB	NB	NB	NM	O	O
PS	NM	NM	NM	NM	O	PS	PS
PO	NM	NM	NS	O	PS	PM	PM
NO	NM	NM	NS	O	PS	PM	PM
NS	NS	NS	O	PM	PM	PM	PM
NM	O	O	PM	PB	PB	PB	PB
NB	O	O	PM	PB	PB	PB	PB

Table 2. Fuzzy rule bases for ESP control.

steering input from the steering wheel and the steering input is set as a step signal with amplitude of 120°. The road excitation is assumed to be independent for the four wheels.

After tuning the parameter setting for the hierarchical control system, we select the weighting parameters for the ASS: $r_1 = r_2 = r_3 = r_4 = 1$, $q_1 = q_2 = q_3 = q_4 = 10^3$, $q_5 = q_6 = q_7 = q_8 = 10^4$, $q_9 = 2 \times 10^3$, $q_{10} = 10^5$, and $q_{11} = 10^6$. Moreover, the weighting parameters for the upper layer controller are selected as: $n_1 = 0.80$ and $n_2 = 0.85$.

The simulation results for the multiple performance indices are shown in Fig. 11 and Fig. 12 (For brevity, only some representative performance indices are presented here).

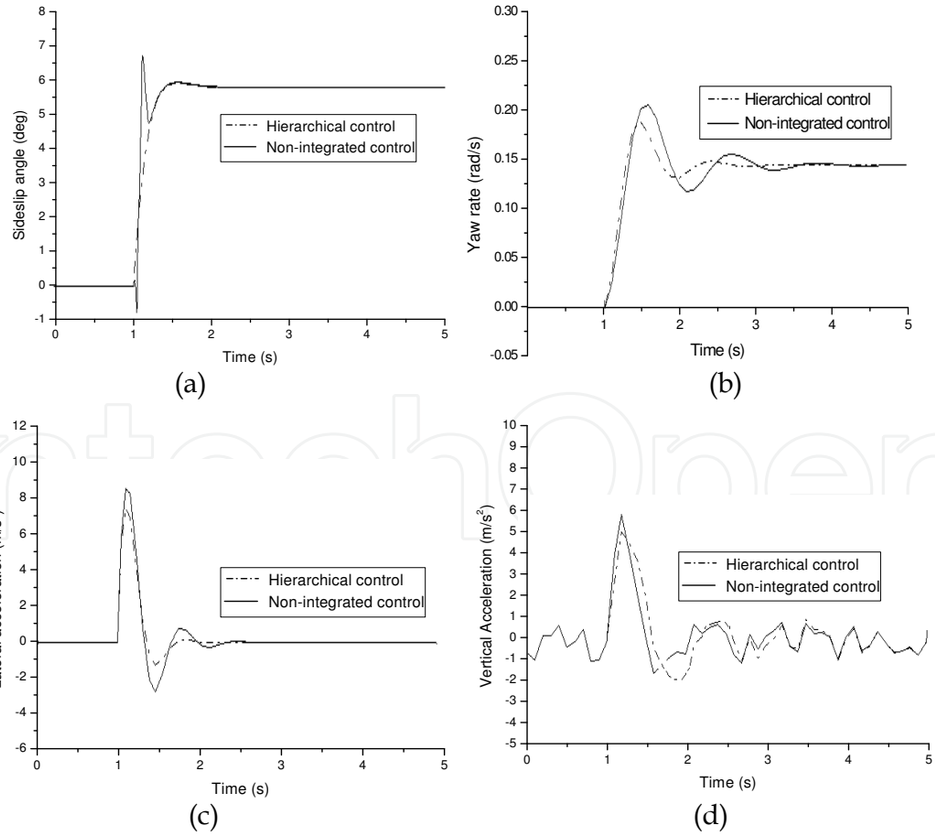

Fig. 11. Comparison of responses for the manoeuvre of step steering input: (a) sideslip angle; (b) yaw rate; (c) lateral acceleration; (d) vertical acceleration.

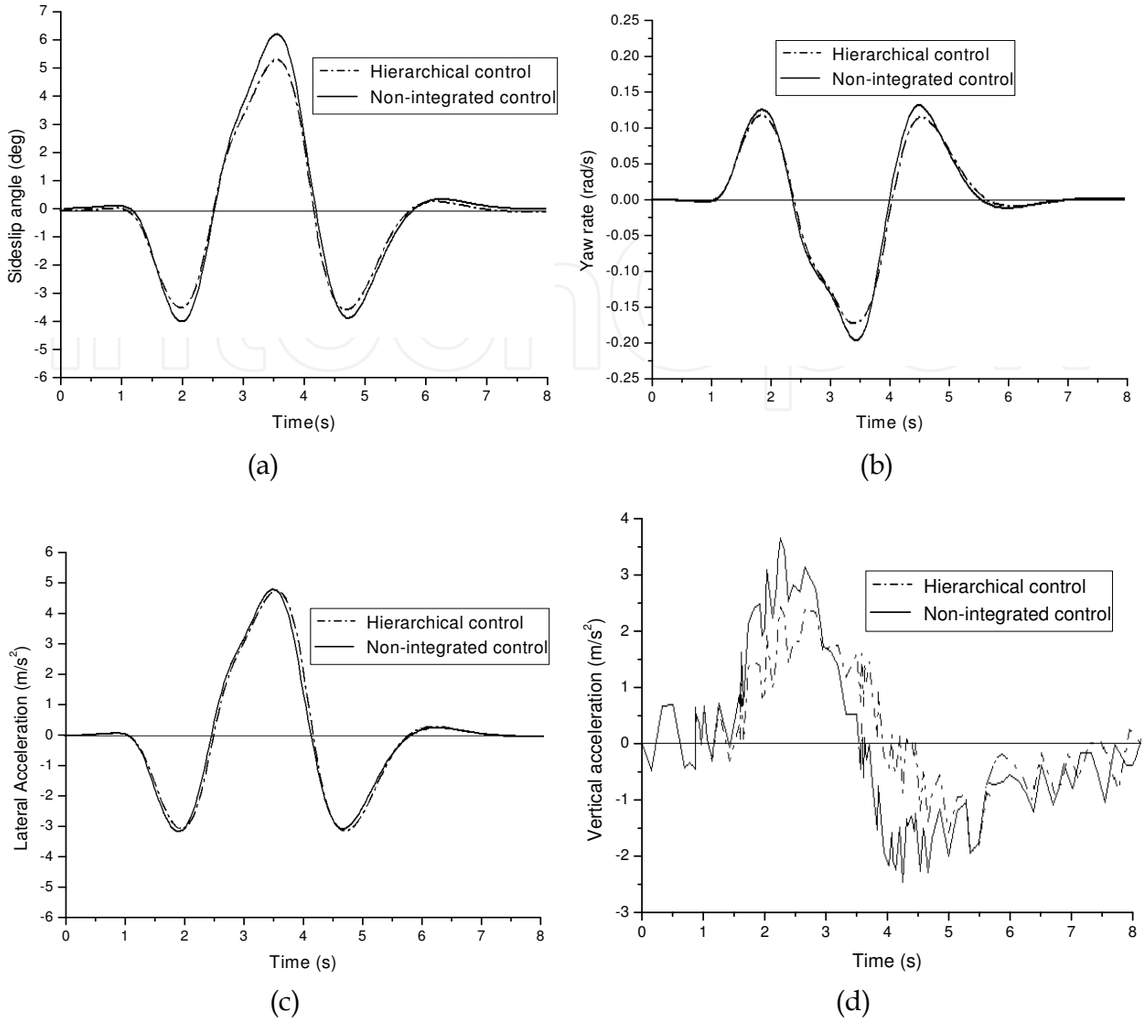

Fig. 12. Comparison of responses for the manoeuvre of double lane change: (a) sideslip angle; (b) yaw rate; (c) lateral acceleration; (d) vertical acceleration.

For comparisons, the simulation investigation for non-integrated control is also performed. In the case, we simply eliminate the upper layer controller. The following discussions are made:

1. For the manoeuvre of step steering input, it can be seen that the peak value of the sideslip angle for hierarchical control, as shown in Fig. 11(a), is reduced by 11.6% compared to that for non-integrated control. Moreover, the sideslip angle for hierarchical control is damped quickly and thus has less oscillation than that for non-integrated control. Similar patterns can be observed for the yaw rate and the lateral acceleration illustrated in Fig. 11(b) and Fig. 11(c), respectively. The results indicate that the vehicle lateral stability is improved by the proposed hierarchical control system in comparison with the non-integrated control system. In addition, the vertical acceleration of sprung mass, one of ride comfort indices, is presented in Fig. 11(d). It can be observed that the peak value of the performance index is decreased by 13.8% for hierarchical control, compared to that for non-integrated control.

2. For the manoeuvre of double lane change, it is observed that the peak value of the sideslip angle for hierarchical control is reduced by 15.3% compared to that for non-integrated control, as shown in Fig. 12(a). Moreover, for the peak value of the yaw rate shown in Fig. 12(b), the percentage of decrease is 7.9. However, as shown in Fig. 12(c), there is no significant difference on the lateral acceleration between the two control cases. While for the vertical acceleration of sprung mass shown in Fig. 12(d), it can be seen clearly that the peak value of this performance index for hierarchical control is reduced significantly by 30.5%, compared to that for non-integrated control. In addition, a quantitative analysis of the vertical acceleration shows that the R.M.S. (Root-Mean-Square) value of the vertical acceleration for hierarchical control is reduced by 21.9% compared to that for non-integrated control.

In summary, the application of the hierarchical control system improves the overall vehicle performance including the ride comfort and the lateral stability under the critical driving conditions. The results show that the hierarchical control system is able to coordinate the interactions between the ASS and the ESP and thus expand the functionalities of the two individual control systems.

5. Investigation 3: Experiment

To verify the effectiveness of the proposed hierarchical control architecture, an experimental study is performed. A physical configuration of the two-layer hierarchical control architecture is illustrated in Fig. 13. The upper layer controller determines the corrective yaw moment to track the desired vehicle motions by using the signals from the CAN-bus, e.g. driver's intentions, environment information, and current vehicle dynamic states. Thereafter, the upper layer controller generates the distributed torques to the two lower layer controllers, i.e., the ESP and the ASS, respectively, according to a rule-based control strategy. Moreover, the distributed torques are converted into the corresponding control commands for the two individual actuators to regulate or track respectively the vehicle dynamic states.

Development and test of complex control systems often benefit from a technique called hardware-in-the-loop (HIL) simulation. The advantages of this technique over real plant tests include: greater flexibility and higher safety in the test scenarios, shorter development time and reduced cost, and measurable/reproducible criteria for system and subsystem evaluation. With those in mind, the HIL simulation is applied to verify the effectiveness of the proposed hierarchical control system. Fig. 14 shows the developed hardware-in-the-loop test platform for the hierarchical control system. The client computer (PXI-8196 by National Instruments Inc.) collects the signals measured by the sensors, which include the pressure of each brake wheel cylinder, the pressure of brake master cylinder, and the vertical acceleration of sprung mass at each suspension, etc. These signals are in turn provided to the host computer (PC) through CAN-bus. Based on these input signals, the host computer computes the vehicle states and the desired vehicle motions, such as the desired yaw rate. Thereafter, the host computer generates control commands to the client computer. Through the hardware interface circuits, the client computer in turn sends the control commands to the corresponding actuators.

The experimental setup is shown in Fig. 15. A test vehicle was equipped with the developed control units for the upper layer controller, ESP controller and ASS controller. The test vehicle was running on a road simulator, which is mounted on the test ground as shown in

the figure. Therefore the road excitation signal can be generated through the road simulator. Again, the two same driving conditions as those used in the simulation investigation were performed, i.e., the manoeuvre of step steering input and the manoeuvre of double lane change. Two cases were tested in the experiment, one is "with hierarchical control", and the other is "non-integrated control". For both testing cases, numerous vehicle tests were performed to validate the developed control units. The measured dynamic responses of the vehicle performance indices are illustrated in Fig. 16 for the manoeuvre of step steering input and Fig. 17 for the manoeuvre of double lane change, respectively.

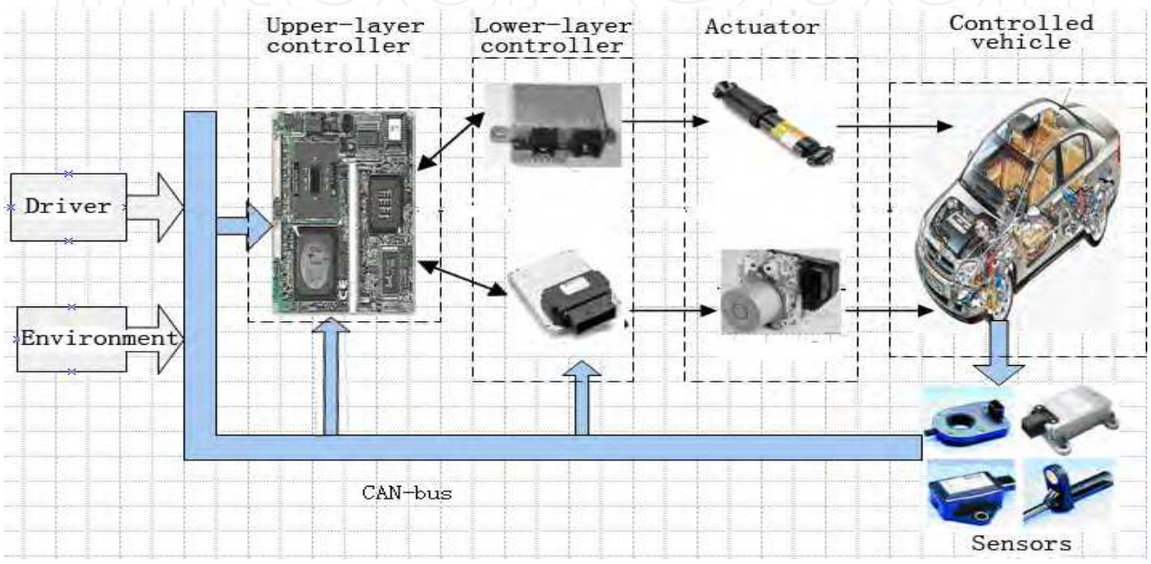

Fig. 13. Physical configuration of the hierarchical control architecture.

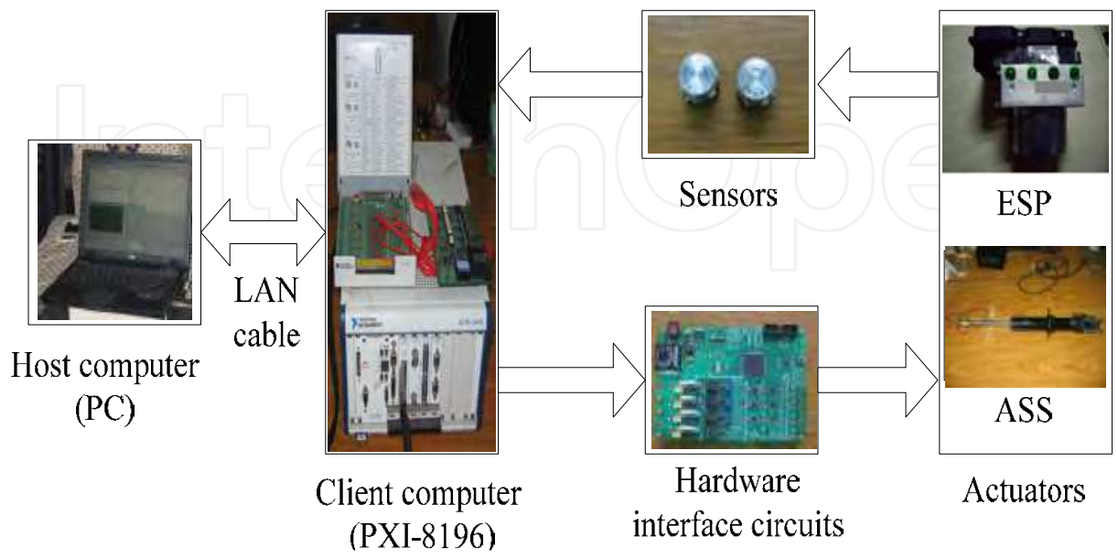

Fig. 14. HIL experimental configuration.

Fig. 15. Experimental setup.

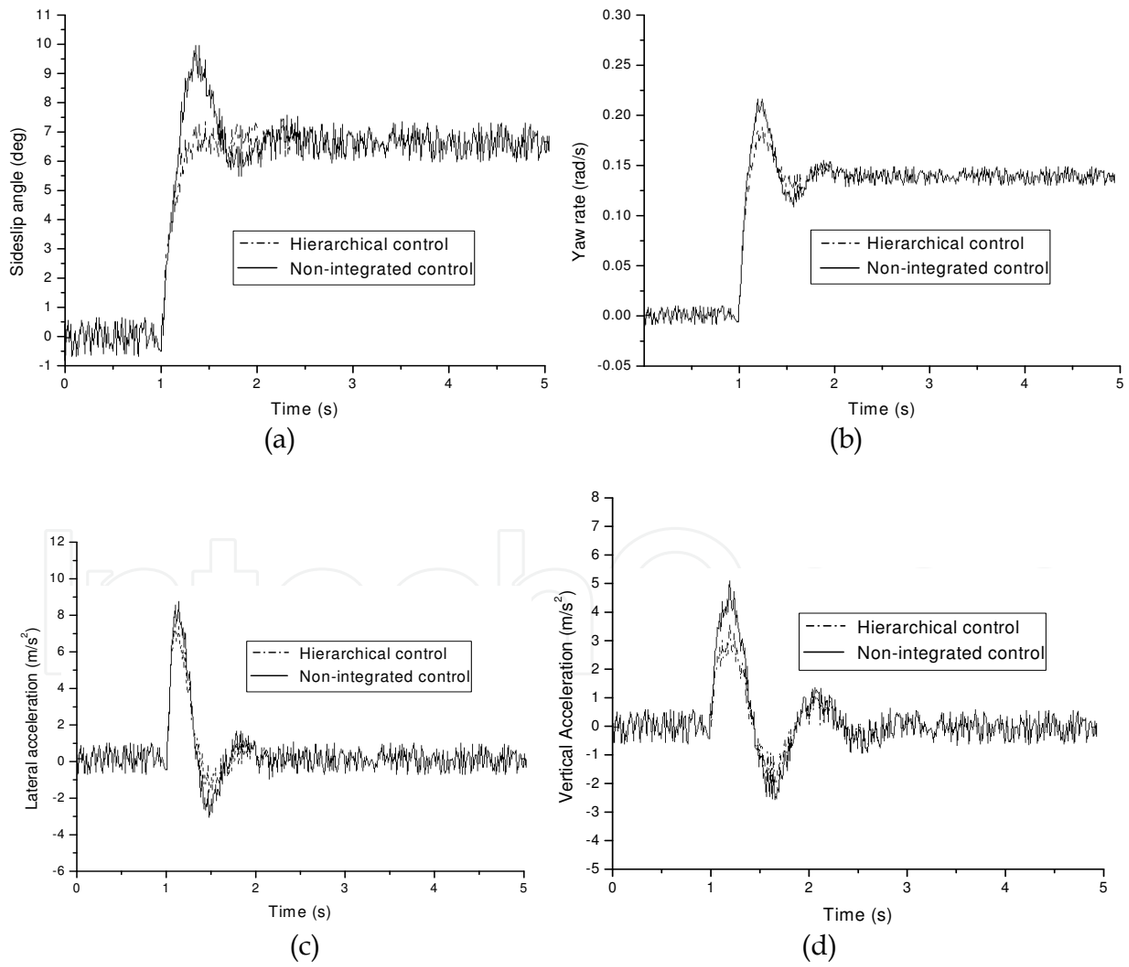

Fig. 16. Comparison of responses for the manoeuvre of step steering input: (a) sideslip angle; (b) yaw rate; (c) lateral acceleration; (d) vertical acceleration.

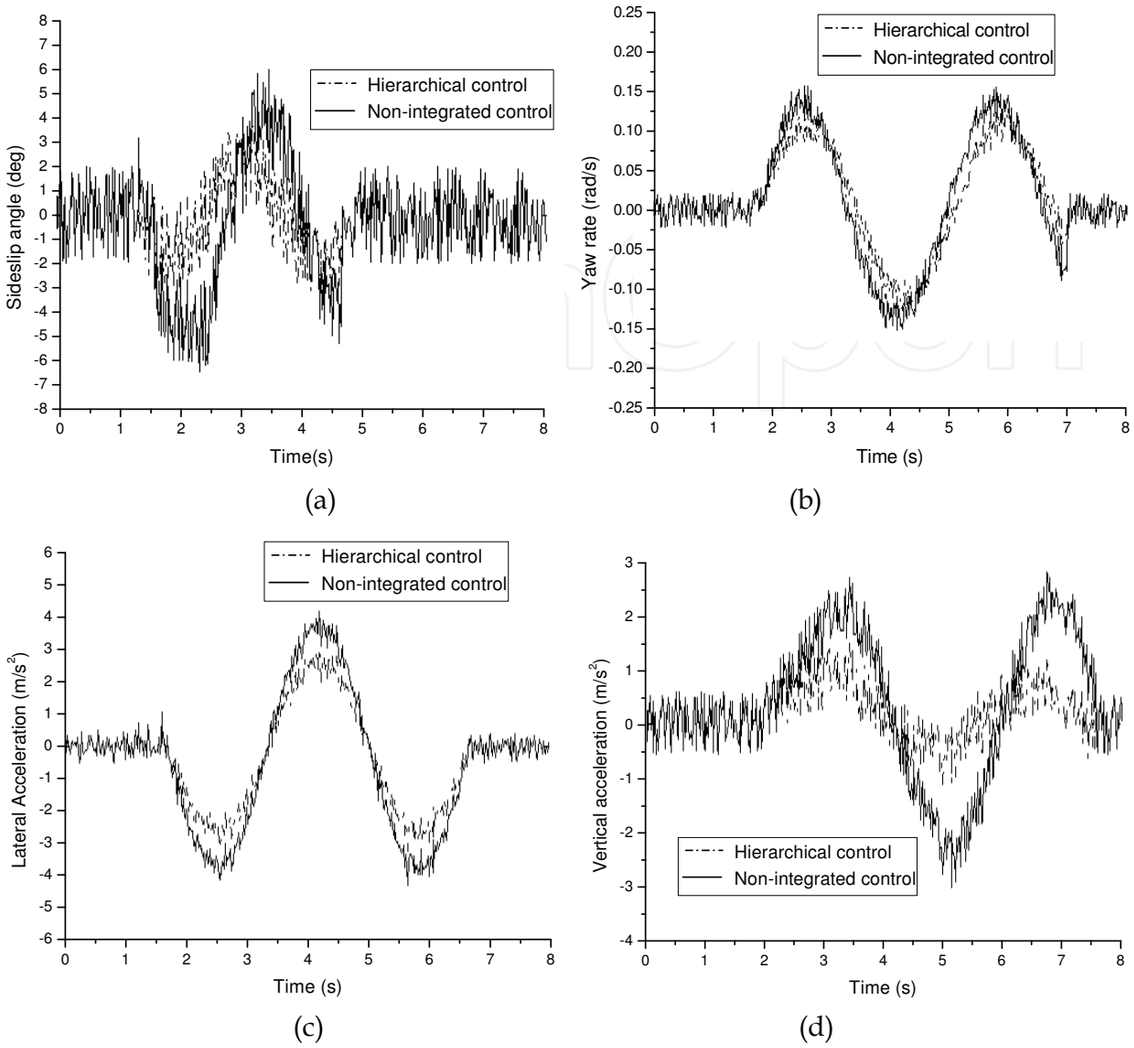

Fig. 17. Comparison of responses for the manoeuvre of double lane change: (a) sideslip angle; (b) yaw rate; (c) lateral acceleration; (d) vertical acceleration.

The following discussions are made by comparing the corresponding performance indices for hierarchical control and non-integrated control:

1. For the manoeuvre of step steering input, it is shown clearly in Fig. 16(a) that the peak value of the sideslip angle for hierarchical control is reduced by 25.1%, compared to that for non-integrated control. The similar phenomena can be observed in Fig. 16(b) for the yaw rate and Fig. 16(c) for the lateral acceleration, except that the percentages of decrease for the two performance indices are slightly smaller than that for the sideslip angle. In addition, as shown in Fig. 16(d), the peak value of the vertical acceleration of sprung mass is decreased greatly by 30.1% for hierarchical control, compared to that for non-integrated control. The results indicate that both the lateral stability and the ride comfort are improved by the proposed hierarchical control system in comparison with the non-integrated control system.
2. For the manoeuvre of double lane change, it is observed in Fig. 17(a) through Fig. 17(c) that the peak values of the sideslip angle, the yaw rate, and the lateral acceleration have

certain amount of decrease for hierarchical control, compared to those for non-integrated control. Moreover, a smaller R.M.S. value can be observed for those performance indices even without calculation. Finally, as presented in Fig. 17(d), the peak value of the vertical acceleration of sprung mass for hierarchical control is reduced significantly by 59.2%, compared to that for non-integrated control. A quantitative analysis of the vertical acceleration shows that the R.M.S. value of the vertical acceleration for hierarchical control is reduced by 47.9% compared to that for non-integrated control.

3. The experimental results have good agreement with the simulation results on demonstrating the vehicle performance improvements by the proposed hierarchical control system.

In summary, the experimental results demonstrate that the proposed hierarchical control system is able to improve both the lateral stability and the ride comfort, in comparison with the non-integrated control system. The experimental results verify the effectiveness of the hierarchical control system.

In the second and third investigations, integrated control and coordination of active suspension system (ASS) and electronic stability program (ESP) have been studied by using hierarchical control strategy. A two-layer hierarchical control architecture has been proposed to achieve the goal of function integration for the two chassis control systems. The upper layer controller has been designed to coordinate the interactions between the ASS and the ESP. A rule-based control method has been used to design the upper layer controller. In addition, the two lower layer controllers including the ASS and the ESP, have been designed independently to achieve their local control objectives. The LQG control strategy and the adaptive fuzzy logic control method have been used to design the ASS and the ESP, respectively. Both a simulation investigation and a hardware-in-the-loop experimental study have been performed. Simulation results demonstrate that the proposed hierarchical control system is able to improve the multiple vehicle performance indices including both the ride comfort and the lateral stability. Moreover, the experimental results verify the effectiveness of the design of the hierarchical control system.

6. Conclusions

In this chapter, integrated control and coordination of vehicle system dynamics have been studied comprehensively and intensively through theoretical developments and experimental verifications. The study consists of three investigations. The first investigation has been focused on coordinating the interactions and function conflicts between the steering system and the suspension system by using a multivariable control approach called stochastic sub-optimal control strategy. Simulation results show that the integrated control system is effective in improving the overall vehicle performance including handling, lateral stability, and ride comfort, compared to either the EPS-only system or the ASS-only system, and the passive system. Moreover, a more advanced integrated control approach called hierarchical control method has been applied to coordinate control of the ASS and the ESP. The design flexibility of the hierarchical control method has been demonstrated through the design practice of the two-layer control system. The upper layer controller has been designed to coordinate specifically the interactions between the ASS and the ESP. While the two lower layer controllers including the ASS and the ESP, have been designed independently to achieve their local control objectives. The application of the hierarchical control method to upper layer controller design has been focused on function coordination

of the two lower layer control systems and thus few modifications are required for the two subsystems, in contrast to the multivariable control approach. Finally, both a simulation investigation and a hardware-in-the-loop experimental study have been performed. Simulation and experimental results demonstrate that the proposed hierarchical control system is able to improve the multiple vehicle performance indices including both the ride comfort and the lateral stability, compared to the non-integrated control system.

7. Acknowledgement

This research was sponsored in part by the Natural Science Foundation of China under Grant No. 51075112, and the Royal Society of UK under Grant No. 16558.

8. Nomenclature

a, b: horizontal distance between the C.G. of the vehicle and the front, rear axle;
$\boldsymbol{A}$, $\boldsymbol{B}$: state matrix, input matrix;
A_w : brake area of the wheel;
c_e : equivalent damping coefficient reflected to the pinion axis;
c_i: damping coefficient of the suspension at wheel i;
c_p: equivalent braking coefficient of the braking system;
c_λ : lateral stiffness of the tyre;
$\boldsymbol{C}$: output matrix;
C_f, C_r: corning stiffnesses of the front tyre and the rear tyre, respectively;
d: half of the wheel track;
de: difference of the yaw rate tracking error;
$\boldsymbol{D}$: feedforward matrix;
e: yaw rate tracking error;
f_0: low cut-off frequency;
$f_1 \sim f_4$: control force of each active suspension controller;
f_r: rolling resistance coefficient;
$F_{x1} \sim F_{x4}$ and $F_{y1} \sim F_{y4}$: longitudinal and lateral forces of the four wheels, respectively;
$F_{z1} \sim F_{z4}$: total force of the suspension acting on the sprung mass;
G_0 : road roughness coefficient;
h: vertical distance between the C.G. of sprung mass and the roll center;
I_p: equivalent moment of inertia of multiple parts reflected to the pinion axis. The multiple parts include the motor, the gear assist mechanism, and the pinion;
I_w: wheel moment of inertia about its spin axis;
I_x, I_y, I_z: roll moment of inertia, pitch moment of inertia, and yaw moment of inertia of sprung mass;
I_{xz}: product of inertia of sprung mass about the roll and yaw axes;
J: performance index;
k_{af}, k_{ar}: stiffness of the anti-roll bars for the front, rear suspension;
k_e, k_{de}: scaling factor;
k_s : torsional stiffness of the torque sensor;
k_{si}: stiffness of the suspension at wheel i;
k_{ti}: stiffness of tyre at wheel i;

k_α : cornering stiffness of the tyre;
K: state feedback gain matrix;
L: wheel base;
m, m_s, m_{ui} : mass of the vehicle, sprung mass, and unsprung mass at wheel i;
M_{ASS}, M_{ESP}: distributed torques for the ASS and the ESP, respectively;
M_d, M_p: braking/traction torque and pitch torque;
M_{ZC}: corrective yaw moment generated by the ESP controller;
n_1, n_2: weighting coefficient;
N: weighting matrix;
N_2: speed reduction ratio of the rack-pinion mechanism;
p_w : pressure of the brake wheel cylinder;
q_1,…, q_{11}, r_1,…, r_4: weighting coefficient;
Q, R: weighting matrix;
R_b: brake radius;
R_w: tyre rolling radius;
S: vehicle stability factor;
T_0: ideal steering torque applied on the steering wheel;
T_c: torque applied on the steering wheel;
T_i: wheel torque at wheel i;
T_m: assist torque applied on the steering column;
T_r: aligning torque transferred from tyres to the pinion;
T_{zwi}: aligning torque acting on the tyre i;
U, $\mathbf{U}_1$, $\mathbf{U}_2$: control input vector, control force vector, and road excitation vector, respectively;.
v, v_x, and v_y: vehicle speed, vehicle speed in the longitudinal direction and the lateral direction, respectively;
w_i : zero-mean Gaussian white noise with intensity of 1;
X, Y: state vector, output vector;
z_{gi}: road excitation;
z_s: vertical displacement of sprung mass;
z_{ui}: vertical displacement of unsprung mass;
α : sideslip angle of the tyre;
β : sideslip angle of the vehicle at the C.G.;
δ_1 : rotation angle of the pinion;
δ_f , δ_r : steering angles of the front, rear wheels;
δ_i : steering angle of wheel i;
ϕ : roll angle of sprung mass;
λ_w : pneumatic trail of the tyre;
μ_b : brake friction coefficient;
θ : pitch angle of sprung mass;
θ_h : rotation angle of the steering wheel;
ω_i : angular velocity of wheel i;
ω_z , ω_{ze} : yaw rate of the vehicle, desired yaw rate of the vehicle;

9. Appendix

The acceleration of the vehicle can be expressed by

$$a = \left(\dot{v}_x - v_y\omega_z\right)i + \left(\dot{v}_y + v_x\omega_z\right)j \tag{a1}$$

where $v_x = v\cos\beta$ and $v_y = v\sin\beta$; the above equation can be derived as the following equation by assuming the vehicle speed v is constant

$$a = -v\left(\dot{\beta} + \omega_z\right)\sin\beta i + v\left(\dot{\beta} + \omega_z\right)\cos\beta j \tag{a2}$$

Therefore

$$a_x = -v\left(\dot{\beta} + \omega_z\right)\sin\beta \tag{a3}$$

$$\text{and} \quad a_y = v\left(\dot{\beta} + \omega_z\right)\cos\beta \tag{a4}$$

and hence

$$a_x\cos\beta = -a_y\sin\beta \tag{a5}$$

Combining Eq. (a3) and (a5), the following equation can be easily derived

$$\dot{\beta} = -\omega_z + \frac{1}{v}(a_y\cos\beta - a_x\sin\beta) \tag{a6}$$

When β is small, the following equation can be easily derived from Eq. (a4)

$$\dot{\beta} = \frac{a_y}{v} - \omega_z \tag{a7}$$

10. References

Bakker, E, Nyborg, L, and Pacejka, H.B. (1987), Tyre Modeling for Use in Vehicle Dynamics Studies, *SAE Technical Paper 870421*, pp. 2190-2198.

Boada, B.L., Boada, M.J.L., and Diaz, V. (2005), Fuzzy-logic Applied to Yaw Moment Control for Vehicle Stability, *Vehicle System Dynamics*, Vol. 43, pp. 753-770.

Chang, S., and Gordon, T.J. (2007), Model-based Predictive Control of Vehicle Dynamics, *International Journal of Vehicle Autonomous Systems*, Vol. 5(1-2), pp. 3-27.

Chen, W.W., Xiao, H.S., Liu, L.Q., and Zu, J.W. (2006), Integrated Control of Automotive Electrical Power Steering and Active Suspension Systems Based on Random Sub-optimal Control, *International Journal of Vehicle Design*, Vol. 42(3/4), pp. 370-391.

Falcone, P., Borrelli, F., Asgari, J., Tseng, H. E., and Hrovat, D. (2007), Predictive Active Steering Control for Autonomous Vehicle Systems, *IEEE Transactions on Control Systems Technology*, Vol. 15(3), pp. 566-580.

Fruechte, R.D., Karmel, A.M., Rillings, J.H., Schilke, N.A., Boustany, N.M., and Repa, B.S. (1989), Integrated Vehicle Control, *Proceedings of the 39th IEEE Vehicular Technology Conference*, Vol. 2, pp. 868-877.

Gordon, T.J. (1996), An Integrated Strategy for the Control of a Full Vehicle Active Suspension System, *Vehicle System Dynamics*. Vol. 25, pp. 229-242.

Gordon, T.J., Howell, M., and Brandao, F. (2003), Integrated Control Methodologies for Road Vehicles, *Vehicle System Dynamics*, Vol. 40(1-3), pp. 157-190.

Gu, Z.Q., Ma, K.G., and Chen, W.D. (1997), *Active Control of Vibration* (in Chinese), China National Defense Industry Press, Beijing, China.

He, J.J., Crolla, D.A., Levesley, M.C., and Manning, W.J. (2006), Coordination of Active Steering, Driveline, and Braking for Integrated Vehicle Dynamics Control, *Proceedings of Institution of Mechanical Engineers - Part D: Journal of Automobile Engineering*, Vol. 220, pp. 1401-1421.

Hirano, Y., Harada, H., Ono, E., and Takanami, K. (1993), Development of An Integrated System of 4WS and 4WD by H Infinity Control, *SAE Technical Paper 930267*, pp. 79-86.

Karbalaei, R., Ghaffari, A., Kazemi, R., and Tabatabaei, S.H. (2007), A New Intelligent Strategy to Integrated Control of AFS/DYC Based on Fuzzy Logic, *International Journal of Mathematical, Physical and Engineering Sciences*, Vol. 1(1), pp. 47-52.

Li, D.F., Du S.Q., and Yu, F. (2008), Integrated Vehicle Chassis Control Based on Direct Yaw Moment, Active Steering, and Active Stabiliser, *Vehicle System Dynamics*, Vol. 46(1), pp. 341-351.

Nwagboso, C. O., Ouyang, X., and Morgan, C. (2002), Development of Neural Network Control of Steer-by-wire System for Intelligent Vehicles, *International Journal of Heavy Vehicle Systems*, Vol. 9(1), pp. 1-26.

Pacejka, H.B. (2002), *Tyre and Vehicle Dynamics*, Butterworth-Heinemann, Boston.

Rodic, A.D., and Vukobratovie, M.K. (2000), Design of an Integrated Active Control System for Road Vehicles Operating with Automated Highway Systems, *International Journal Computer Application Technology*, Vol. 13, pp. 78-92.

Trächtler, A. (2004), Integrated Vehicle Dynamics Control Using Active Brake, Steering, and Suspension Systems, *International Journal of Vehicle Design*, Vol. 36(1), pp. 1-12.

Yu F., and Crolla D.A. (1998), An Optimal Self-tuning Controller for An Active Suspension, *Vehicle System Dynamic*, Vol. 29, pp. 51-65.

Yu, F., Li, D.F., Crolla, D.A. (2008), Integrated Vehicle Dynamic Control – State-of-the Art Review, *Proceedings of IEEE Vehicle Power and Propulsion Conference (VPPC)*, September 3-5, Harbin, China, pp. 1-6.

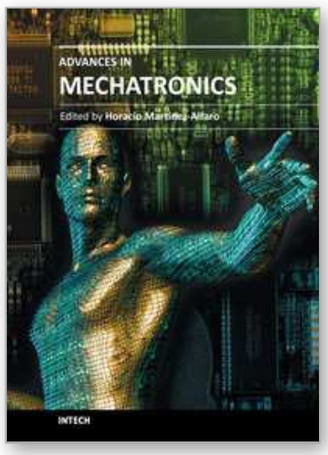

Advances in Mechatronics

Edited by Prof. Horacio Martinez-Alfaro

ISBN 978-953-307-373-6
Hard cover, 300 pages
Publisher InTech
Published online 29, August, 2011
Published in print edition August, 2011

Numerous books have already been published specializing in one of the well known areas that comprise Mechatronics: mechanical engineering, electronic control and systems. The goal of this book is to collect state-of-the-art contributions that discuss recent developments which show a more coherent synergistic integration between the mentioned areas.Â Â The book is divided in three sections. The first section, divided into five chapters, deals with Automatic Control and Artificial Intelligence. The second section discusses Robotics and Vision with six chapters, and the third section considers Other Applications and Theory with two chapters.

How to reference

In order to correctly reference this scholarly work, feel free to copy and paste the following:

Wuwei Chen, Hansong Xiao, Liqiang Liu, Jean W. Zu and HuiHui Zhou (2011). Integrated Control of Vehicle System Dynamics: Theory and Experiment, Advances in Mechatronics, Prof. Horacio Martinez-Alfaro (Ed.), ISBN: 978-953-307-373-6, InTech, Available from: http://www.intechopen.com/books/advances-in-mechatronics/integrated-control-of-vehicle-system-dynamics-theory-and-experiment

INTECH
open science | open minds

InTech Europe
University Campus STeP Ri
Slavka Krautzeka 83/A
51000 Rijeka, Croatia
Phone: +385 (51) 770 447
Fax: +385 (51) 686 166
www.intechopen.com

InTech China
Unit 405, Office Block, Hotel Equatorial Shanghai
No.65, Yan An Road (West), Shanghai, 200040, China
中国上海市延安西路65号上海国际贵都大饭店办公楼405单元
Phone: +86-21-62489820
Fax: +86-21-62489821

© 2011 The Author(s). Licensee IntechOpen. This chapter is distributed under the terms of the Creative Commons Attribution-NonCommercial-ShareAlike-3.0 License, which permits use, distribution and reproduction for non-commercial purposes, provided the original is properly cited and derivative works building on this content are distributed under the same license.

IntechOpen

IntechOpen